

Inhaled Nitric Oxide Preserves Ventricular Function During Resuscitation Using a Percutaneous Mechanical Circulatory Support Device in a Porcine Cardiac Arrest Model – An Echocardiographic Myocardial Work Analysis

Christoph Nix

Abiomed Europe GmbH

Rashad Zayat (✉ r.zayat@gmail.com)

Universitätsklinikum Aachen: Universitätsklinikum Aachen <https://orcid.org/0000-0003-2243-8743>

Andreas Ebeling

RWTH University Hospital: RWTH University Aachen Faculty of Medicine

Andreas Goetzenich

Abiomed Europe GmbH

Uma Chandrasekaran

AbioMed Inc

Rolf Rossaint

RWTH University Hospital: RWTH Aachen University Faculty of Medicine

Nima Hatam

RWTH University Hospital: RWTH Aachen University Faculty of Medicine

Matthias Derwall

RWTH University Hospital: RWTH Aachen University Faculty of Medicine

Research

Keywords: Left ventricular assist device, Percutaneous mechanical circulatory support, Cardiac arrest, Cardiopulmonary resuscitation, Left ventricular unloading, Nitric oxide, Impella

Posted Date: December 1st, 2020

DOI: <https://doi.org/10.21203/rs.3.rs-115076/v1>

License: © ⓘ This work is licensed under a Creative Commons Attribution 4.0 International License.

[Read Full License](#)

Abstract

Background

Resuscitation using a percutaneous mechanical circulatory support device (iCPR) improves survival after cardiac arrest (CA). We hypothesized that the addition of inhaled nitric oxide (iNO) during iCPR might prove synergistic, leading to improved myocardial performance due to lowering of right ventricular (RV) afterload, left ventricular (LV) preload, and myocardial energetics. This study aimed to characterize the changes in LV and RV function and global myocardial work indices (GWI) following iCPR, both with and without iNO, using 2-D transesophageal echocardiography (TEE) and GWI evaluation as a novel non-invasive measurement.

Methods

In 10 pigs, iCPR was initiated following electrically-induced CA and 10min of untreated ventricular fibrillation (VF). Pigs were randomized to either 20ppm (*20ppm*, n=5) or 0ppm (*0ppm*, n=5) of iNO in addition to therapeutic hypothermia for 5h following ROSC. All animals received TEE at five pre-specified time-points and invasive hemodynamic monitoring.

Results

LV end-diastolic volume (LVEDV) increased significantly in both groups following CA. iCPR alone led to significant LV unloading at 5h post-ROSC with LVEDV values reaching baseline values in both groups (*20ppm*: 68.2 ± 2.7 vs. 70.8 ± 6.1 mL, $p=0.486$; *0ppm*: 70.8 ± 1.3 vs. 72.3 ± 4.2 mL, $p=0.813$, respectively). LV global longitudinal strain (GLS) increased in both groups following CA. LV-GLS recovered significantly better in the 20ppm group at 5h post-ROSC (*20ppm*: $-18 \pm 3\%$ vs. *0ppm*: $-13 \pm 2\%$, $p=0.025$). LV-GWI decreased in both groups after CA with no difference between the groups. Within *0ppm* group, LV-GWI decreased significantly at 5h post-ROSC compared to baseline ($1,125 \pm 214$ vs. $1,835 \pm 305$ mmHg%, $p=0.011$). RV-GWI was higher in the *20ppm* group at 3h and 5h post-ROSC (*20ppm*: 189 ± 43 vs. *0ppm*: 108 ± 22 mmHg%, $p=0.049$ and *20ppm*: 261 ± 54 vs. *0ppm*: 152 ± 42 mmHg%, $p=0.041$). The blood flow calculated by the Impella controller following iCPR initiation correlated well with the pulsed-wave Doppler (PWD) derived pulmonary flow (PWD vs. controller: 1.8 ± 0.2 vs. 1.9 ± 0.2 L/min, $r=0.85$, $p=0.012$).

Conclusions

iCPR after CA provided sufficient unloading and preservation of the LV systolic function by improving LV-GWI recovery. The addition of iNO to iCPR enabled better preservation of the RV-function as determined by better RV-GWI. Additionally, Impella-derived flow provided an accurate measure of total flow during iCPR.

Background

Cardiac arrest (CA) remains associated with high mortality and poor functional outcome. Despite the growing clinical use of mechanical circulatory support (MCS) for cardio-pulmonary resuscitation (CPR) after CA, the contribution towards a higher survival rate and the better functional outcome is yet to be demonstrated. An animal study showed a beneficial effect of the early use of a percutaneous mechanical circulatory support device, termed intravascular CPR (iCPR), on post-CPR survival [1]. An additional inhaled nitric oxide (iNO) application in an animal model resulted in improved trans-pulmonary blood flow and was associated with improved neurological outcomes [2]. We hypothesized that the synergistic effects of iNO during iCPR were a result of improved myocardial performance due to lowering of right ventricular (RV) afterload, left ventricular (LV) preload, and myocardial energetics. Previous studies have demonstrated a cardio-protective effect of ventricular unloading by percutaneous MCS through reduction in myocardial wall stress and myocardial work (MW) [3]. Recently, echocardiographic MW assessment has emerged as a non-invasive method to evaluate myocardial performance and gain more insights into myocardial energetics and mechanics, given the strong correlation with invasive pressure-volume (PV) measurements [4].

Thus, in the present study, we aimed to better understand the effect of iNO during iCPR on the myocardial performance and mechanics in a well-established large animal model of CA [1, 2]. The left (LV) and right ventricular (RV) function before, during, and after iCPR were analyzed using 2-D transesophageal echocardiography (TEE), deformation imaging, tissue Doppler (TDI) and non-invasive myocardial work measurement. In addition, trans-pulmonary flow (TPF) inferred by pulsed-wave Doppler (PWD) during iCPR was compared to the calculated pump flow derived from the Impella controller.

Methods

The experimental protocol was approved by the appropriate governmental institution (Landesamt für Natur, Umwelt und Verbraucherschutz NRW (LANUV), Recklinghausen, Germany) and has been previously described [1, 2]. All animals received adequate care according to the precepts of the Helsinki declaration. Ten healthy female swine (Deutsche Landrasse, *Sus scrofa domesticus*), approximately four months of age, and weighing 44 to 57 kg were used in this study. All pigs had a clinical examination on arrival at the facility. Animals were housed in pens with a 12 h-day-night cycle and access to drinking water ad libitum. Twelve hours before the experiment, the pigs were set on nil per os except for drinking water access.

Animal instrumentation

Figure 1 provides an overview of animal instrumentation and the experiment model. The pigs were weighed before the start of the experiment. General anesthesia was induced by intramuscular injection of 4 mg/kg azaperone (Stresnil, Janssen-Cilag GmbH, Neuss, Germany), followed by intravenous injection of 15 mg/kg sodium pentobarbital (Nacoren, Boehringer Ingelheim Vetmedica GmbH, Ingelheim am Rhein, Germany). Anesthesia was maintained by continuous intravenous sodium pentobarbital infusion at a rate of 4 mg/kg/h. The pigs were placed in a supine position, intubated orotracheally, and the legs were fixed in an extended position. Animals were ventilated with an inspired oxygen fraction of 0.3 (Servo

Ventilator 300A; Siemens AG, Munich, Germany). Tidal volume was set to 10 ml/kg, and respiratory rate was adjusted to keep the end-tidal carbon dioxide partial pressure within a physiologic range (35 ± 4 mmHg). A continuous five lead electrocardiogram (ECG) and pulse oximetry were performed. Convective air heating was used to maintain body temperature at $38\pm 0.5^\circ\text{C}$ during preparation (Warm Touch 5200; Tyco Healthcare, Pleasanton, CA, USA).

Hemodynamic monitoring

Arterial blood pressure was obtained using a fluid-filled catheter (Vygon, Ecquen, France) placed into the left femoral artery. For pulmonary artery pressure and cardiac output measurements, a Swan-Ganz catheter (744HF75; Edwards Lifesciences, Irvine, CA, USA) was flow-directed into the pulmonary artery and connected to a cardiac output monitor (Vigilance; Edward Lifesciences). Impella flow was taken from the motor current based flow calculation on the AIC (Automated Impella Controller) as described in detail earlier [5].

Cardiac arrest model

As described previously [1, 2], cardiac arrest was induced using an alternating current of 1 to 2 mA delivered to the endocardium of the right ventricle, resulting in VF. Simultaneously, mechanical ventilation was discontinued.

A 13-French sheath introducer (Impella 2.5 introducer kit 13 F, 13 cm; Abiomed Europe GmbH, Aachen, Germany) was placed in the right femoral artery. A modified Impella 2.5 left ventricular assist device (Abiomed) equipped with a shortened angled cannula to meet the anatomical constraints of the animal was introduced using the vascular access into the left ventricle with the help of fluoroscopy guidance, pigtail catheter (Cordis 6 F PIG 145° 110 cm Super Torque Plus; Cordis, Miami Lakes, FL, USA) and a guidewire (Platinum Plus 0.018 in \times 260 cm; Boston Scientific, Natick, MA, USA) (see Figure 1 for details).

Impella 2.5 support was activated at the maximum achievable flow ten minutes following the onset of VF. The pig was then randomized (closed envelope method) to a FiO_2 of 1.0 without any added iNO (group *0ppm*; $n=5$) versus a FiO_2 of 1.0 blended with 20ppm of inhaled nitric oxide (group *20ppm*; $n=5$). Therapeutic mild hypothermia was induced using 0.5L of a 6°C cold Ringer's solution and topical application of ice bags to the groins in all animals. The blood temperature was maintained at $33\pm 1^\circ\text{C}$. A continuous infusion of Ringer's solution was administered at 4 ml/kg/h to ensure adequate hydration.

Transesophageal Echocardiography

All TEE studies were performed by the same board-certified physician at baseline (after all catheters were placed), during VF and iCPR, and at 30mins, 3h, 5h post-ROSC. We used a commercially available ultrasound machine (Vivid E9, GE Vingmed Ultrasound AS, Horten, Norway) equipped with a 6VT-D [3.0-8.0MHz] TEE probe. Our detailed TEE protocol in swine has been described previously [6]. In brief, at least three consecutive cardiac cycles were stored and averaged for all measurements. The analysis was

carried out offline using the device's software package (EchoPAC Version 202; GE Vingmed Ultrasound AS, Horten, Norway) according to the recommendation of the European Association of Cardiovascular imaging [7]. Images were acquired from mid-esophageal, trans-gastric, and upper esophageal views. Valvular pathologies were excluded by color-Doppler. LV end-diastolic (LVEDV) and end-systolic (LVESV) volumes were measured in the mid-esophageal four-chamber (4-CH) views and deep esophageal two-chamber (2-CH) views. The modified biplane Simpson's method was used for Ejection fraction (EF) measurements [8]. RV fractional area change (RV-FAC) was determined according to the following formula:

$$\text{RV-FAC} = \frac{\text{end-diastolic area} - \text{end-systolic area}}{\text{end-diastolic area}} \times 100\%$$

TDI was used to measure RV peak systolic tricuspid annulus velocity (TASV) from a 4-CH view as an indicator of RV longitudinal function [9]. The PWD sample was placed in RV- (RVOT) and LV-outflow tracts (LVOT) to obtain velocity time integrals (VTI). RV Cardiac output (CO) was calculated using the formula: $\text{CO} = \text{VTI}_{\text{RVOT}} \times \text{RVOT cross-sectional area} \times \text{heart rate}$ and for the LV $\text{CO} = \text{VTI}_{\text{LVOT}} \times \text{LVOT cross-sectional area} \times \text{heart rate}$.

Speckle tracking and non-invasive myocardial work measurements:

2-D speckle-tracking (STE) was used to define LV global longitudinal strain (LV-GLS) and RV-GLS. LV GLS was measured using the three apical chamber views (4-CH, 2-CH and apical long axis (LAX)). For STE analysis of the RV the 4CH view for the RV anterior wall was used. The RV free wall was captured from a modified upper long axis view (LAX) of the RV in- and outflow tract and part of the posterior RVOT was obtained from a mid-esophageal LAX RV view (Please refer to supplementary figure 1 for a representative view). Aortic and mitral valve opening and closure times were determined by PWD. The systolic arterial and pulmonary blood pressures were entered into the EchoPAC software (GE Vingmed Ultrasound AS, Horten, Norway). After completing the STE analysis of LV and RV, EchoPAC calculated pressure-strain loops (PSL). Adjusted LV pressure curves corresponding to the length of isovolumic and ejection phases were generated by EchoPAC software, as described by Russel et al. [10, 11]. The global myocardial work index (GWI) was calculated from the area within the PSL and the following parameters were then calculated from the PSL: 1) GWI: The total myocardial work from mitral valve closure to mitral valve opening is represented by the total area of PSL; 2) global constructive myocardial work (GCW): the ventricular work which contributes to the ejection during systole: $\text{GCW} = \text{positive work during systole} + \text{negative work during isovolumic relaxation}$; 3) global wasted myocardial work (GWW): the ventricular work that does not contribute to the ejection of blood. $\text{GWW} = \text{negative work during systole} + \text{positive work during isovolumic relaxation}$; 4) global myocardial work efficiency (GWE): the fraction of constructive myocardial work to total work [10-12]. LV pressure was estimated by adjusting a reference pressure curve with measured blood pressure and with echocardiography derived valvular event timing [10-12]. We used the blood pressure taken from the femoral artery for that purpose. RV's pressure was measured using the Swan-Ganz catheter. The myocardial work was expressed in mmHg%. EchoPAC

provided a validated assessment of LV myocardial work indices. To our knowledge, measurements for RV myocardial work indices with EchoPAC were not validated by GE healthcare or by any other research group yet.

Statistical analysis

Statistical analysis was performed with STATA IC16 (StataCorp., TX, USA) and Jamovi project (Version 1.6.1, <https://www.jamovi.org>). Figures were created using Graph Pad Prism version 7.0a for MAC OS X (Graph Pad Software, La Jolla, California USA) and prepared for submission using Adobe® Illustrator® CS6 (Adobe Inc., San Jose, California, USA). The normal distribution of continuous variables was assessed using the Shapiro-Wilk-Test, and was expressed as mean \pm standard deviation. A mixed-effects model was used for between-group comparisons at different time-points and Sidak's test was used to account for multiple comparisons. The non-parametric Friedman-test and Dunn's correction for multiple comparisons was used for intergroup comparisons at different time points. Pearson's correlation test was performed to assess the correlation between the invasive thermodilution measured CO (CO_{TD}) and the PWD derived CO (CO_{PWD}). Adjusted p-values for multiple comparisons are presented and $p < 0.05$ was considered statistically significant.

Results

Impella controller derived flow correlates well with pulsed-wave Doppler derived flow

All 10 pigs survived 15h post-ROSC and were successfully extubated. No complications due to TEE probe insertion or during TEE image acquisition were observed. Body surface area was similar between groups (*0ppm*: 1.2 ± 0.1 vs. *20ppm*: 1.3 ± 0.1 m², $p = 0.278$). At least two different clear views of 4-CH, 2-CH, and LAX at all given time points were obtained in all animals.

The mean heart rate at baseline was 92 ± 14 min⁻¹. The systemic and pulmonary artery pressure at baseline did not differ between groups and are presented in Table 1. CO_{PWD} correlated well with the invasively measured CO_{TD} at baseline, 30min, 3h and 5h ($r = 0.71$, $p = 0.021$; $r = 0.91$, $p < 0.001$; $r = 0.93$, $p < 0.001$; $r = 0.84$, $p < 0.01$, respectively) (Figure 2). The calculated pump flow displayed by the automated Impella controller correlated well with the PWD derived pulmonary flow following iCPR initiation (1.8 ± 0.2 vs. 1.9 ± 0.2 L/min, $r = 0.85$, $p = 0.012$).

Application of iNO significantly increases cardiac output and improves left ventricular systolic function recovery

At baseline, LVEDV, LV-EF and LV-GLS did not differ between groups. After induction of VF, LVEDV increased significantly in both groups compared to baseline (Figure 3A). Over the course of iCPR for 5 hours, LVEDV decreased and returned closer to baseline values in both groups (Figure 3A and Table 2). However, LVEDV in the 20ppm group was higher at all time points and was statistically significant at 3h post-ROSC (*0ppm*: 78.2 ± 1.1 vs. *20ppm*: 70.8 ± 1.3 mL, $p < 0.001$). LV-EF did not differ significantly between

groups at all time points or within each group compared to baseline (Figure 3B). The LV-GLS improved throughout the duration of iCPR in both groups from baseline (Figure 3C). The LV-GLS values were significantly lower at 3h and 5h post-ROSC in the *20ppm* group compared to the *0ppm* group (5h: *0ppm*: -13.1 ± 2.4 vs. *20ppm*: -18.2 ± 3.4 , $p=0.025$) (Figure 3C). The CO decreased in both groups at iCPR initiation and improved over the course of iCPR. The CO_{PWD} increased significantly in the *20ppm* group at 3h and 5h post-ROSC compared to the *0ppm* group (3h: *0ppm*: 4.6 ± 0.9 L/min vs. *20ppm*: 6.6 ± 1.1 , $p=0.016$; 5h: *0ppm*: 4.0 ± 0.6 L/min vs. *20ppm*: 5.8 ± 1.0 , $p=0.036$) (Figure 3D).

Application of iNO enhances right ventricular systolic function recovery

RV echocardiographic measurements, RV basal diameters at end-diastole (RVEDD), RV-FAC, TASV and RV-GLS, did not differ between the two groups at baseline (Figure 4A-D and Table 2). However, RV-FAC decreased significantly during CA and 30min post-ROSC. In the *0ppm* group, RV-FAC was lower at all time-points compared to baseline (*0ppm* baseline vs. 30min, vs. 3h vs. 5h post-ROSC: $44.1 \pm 6.1\%$ vs. $27.4 \pm 2.8\%$, $p=0.004$; vs. $32 \pm 5\%$, $p=0.009$; vs. $33.2 \pm 4.3\%$, $p=0.001$; see also table 2). In the *20ppm* group, RV-FAC improved at 3h and recovered to baseline values at 5h post-ROSC (baseline: $42.9 \pm 6.6\%$ vs. 5h: 41.1 ± 6.4 ; $p=0.442$) (Figure 4A). RVEDD increased significantly in both groups at iCPR initiation, and slowly recovered over time but did not differ between groups (Figure 4B and Table 2). Within the *0ppm* group, TASV decreased significantly after CA and remained lower during the course of iCPR (baseline vs. 3h: 13.6 ± 1.1 vs. 7.8 ± 1.6 cm/s, $p=0.024$; baseline vs. 5h: 13.6 ± 1.1 vs. 9.4 ± 1.3 cm/s, $p=0.009$, respectively) (Figure 4A and Table 2). The TASV values in the *20ppm* group were higher at 3h and 5h post-ROSC compared to the *0ppm* group (*20ppm* vs. *0ppm* at 3h: 11.4 ± 1.1 vs. 7.8 ± 1.6 cm/s, $p=0.024$; at 5h: 12.8 ± 1.1 vs. 9.4 ± 1.3 cm/s, $p=0.012$). The RV-GLS values were similar between the two groups at baseline and post-ROSC. However, RV-GLS at 5h post-ROSC was significantly lower in the *20ppm* group than *0ppm* (*0ppm* vs. *20ppm* at 5h: $-9 \pm 1.4\%$ vs. $-13 \pm 2.2\%$; $p=0.007$; Figure 4D).

LV myocardial work indices indicate recovery during and after ventricular unloading

At baseline, myocardial work indices (GWI, GWE, GCW, GWW) did not differ between the two groups (Figure 5A-D and Table 2). The LV-GWI did not differ between the two groups at any time. However, LV-GWI in the *20ppm* group recovered after an initial decrease and began to recover at 30min post-ROSC to reach almost baseline values at 5h post-ROSC (baseline: $1,751 \pm 270$ mmHg% vs. 5h: $1,529 \pm 274$ mmHg%, $p=0.401$) (Figure 5A and Table 2), while in the *0ppm* group, LV-GWI was significantly lower compared to baseline at all time-points (baseline: $1,835 \pm 305$ mmHg%; 30min: 891.2 ± 412 mmHg% ($p=0.032$), 3h: 896 ± 129 mmHg% ($p=0.011$), and 5h: $1,125 \pm 214$ mmHg% ($p=0.011$); Figure 5A). LV-GWE and LV-GCW had a similar time-course to LV-GWI and did not recover in the *0ppm* group (Figure 5B). The LV-GWW did not differ between groups and did not increase significantly in both groups at all time-points compared to baseline (Figure 5C).

RV myocardial indices indicate a more complex pattern and slower recovery

At baseline, the RV myocardial work indices did not differ between groups (*0ppm* vs. *20ppm*, Figure 6A-C and Table 2). At 3h and 5h post-ROSC, RV-GWI was significantly lower in the *0ppm* group compared to the *20ppm* group (*0ppm*: 108.4 ± 22.6 vs. *20ppm*: 189.6 ± 43.6 mmHg%, $p=0.049$ and *0ppm*: 152.6 ± 42.4 vs. 261.6 ± 54.2 mmHg%, $p=0.041$, respectively). Within the *0ppm* group, the RV-GWI did not recover and remained significantly decreased at 30min, 3h and 5h post-ROSC compared to baseline (baseline: 338.2 ± 45.3 mmHg% vs. 30min: 101.6 ± 34.5 mmHg%, $p<0.001$; vs. 3h: 108.4 ± 22.6 mmHg%, $p<0.001$; vs. 5h: 152.6 ± 42.4 mmHg%, $p=0.012$, respectively; Figure 6B). In both groups, the RV-GCW decreased significantly after CA, but a slow recovery over time was noted in both groups with no difference between groups (Figure 6B and Table 2). The RV-GWW increased significantly in the *0ppm* group compared to the *20ppm* group at 3h and 5h post-ROSC: 69.6 ± 11.9 vs. 47.4 ± 6.7 , $p=0.049$ and 77.8 ± 14.8 vs. 50.2 ± 8.2 , $p=0.046$, respectively (Figure 6C). The RV-GWE increased significantly in the *20ppm* group at 5h post-ROSC compared to the *0ppm* group (80 ± 5.2 vs. 73 ± 5.7 , $p=0.042$, respectively)

Diagnostic utilization of pressure-strain loops

Figure 7A is a representative overlay of the PS-loops of the LV. An acute injury following iCPR initiation is demonstrated by narrowing of the PS-loop (a sign of loss in maximally generated strain), thus explaining the ventricle's inability to generate sufficient pressure [13-17].

The partially positive strain indicates a passive distention of the myocardium due to volume loading [15-17]. Unloading leads to slow recovery and progressive normalization of the PS-loop, which remains below (i.e., less negative) normal values but shows a curve pattern comparable to normal conditions [17, 18].

Figure 7B is a representative overlay of the PS-loops of the right ventricle. A pumping failure leads to increased RVP, and a loss in strain translates to a more complex strain-pressure relation [19, 20]. The RV strain reduction remains pronounced even after a longer duration of left ventricular support [20, 21].

Figure 7C demonstrates the spatial distribution of strain at different time-points. This allows differentiation of regional wall motion deterioration e.g., in acute myocardial infarction from global failure, thus providing a detailed perspective on myocardial recovery over time.

Discussion

Resuscitation following cardiac arrest remains associated with significant mortality and morbidity [22]. Although treatment guidelines recommend inotropes and vasopressors, many studies have demonstrated their detrimental side effects [22]. In the early phase of resuscitation, treatments aim to augment or stabilize cardiac output, allowing minimal end-organ perfusion, and reducing or preventing hypoxic/ischemic injury [12-14]. However, these treatments cause increased myocardial stress and oxygen demand when oxygen supply is low [23, 24].

Trans-valvular mechanical support devices like the Impella device family uncouple the myocardial workload from the systemic cardiac output (which is then primarily provided by the pump), leading to

adequate end-organ perfusion while resting the heart [3, 25]. Previous studies [26-28] have demonstrated the efficacy of this intravascular resuscitation, and the present study in an animal model confirms the results and provides additional insights on the temporal evolution of the effect.

Global myocardial work and the principle of unloading

The pressure-strain (PS) loop generated by tracking the global myocardial strain vs. the LVEDP/RVEDP over the cardiac cycle provides a momentary impression of the myocardial work and is comparable to the pressure-volume (PV) loops derived from conductance catheters [4, 10, 11]. Russel et al. [10, 11] demonstrated a strong correlation between the non-invasive LV PS-loop area and the invasive PV-loop area. The LV PV-loop analysis considers the LV load and has been shown in experimental studies to be a reliable and robust method for quantifying LV performance. Moreover, the PV-loop area provides valuable information on the myocardial O₂-consumption [29, 30]. Despite being a valuable and reliable method, the PV-loop method is not used in clinical practice due to its invasiveness [10, 11, 31, 32].

Evaluation of ventricular function is an essential component of all echocardiographic examinations. Despite the many LVEF measurement limitations, LVEF remains the most widely used parameter for systolic function evaluation [33]. More recently, the peak longitudinal strain from 2D-speckle tracking analysis has gained acceptance in the clinical routine. Compared to EF, GLS can detect subclinical myocardial abnormalities. However, GLS analysis suffers from load dependency and has limitations [34].

The PS-loop analysis incorporates both the deformation changes and afterload, thus overcoming the limitations of load dependency [4]. Therefore, GWI provides incremental information to EF and GLS analysis. While the PV-loop area reflects myocardial metabolic demand and oxygen consumption, the non-invasive myocardial work method provides myocardial energetics [10, 11, 32]. For several decades, stroke work evaluation played a key role in heart failure characterization and decision-making regarding optimal treatment. Traditional stroke work measurements are calculated using the LV PV-loop area derived from invasive catheterization [29, 30]. The PS-loop method has a robust correlation with invasive PV-loops and enables evaluating myocardial wasted work and work efficiency [11]. The value and clinical implications of non-invasively estimated myocardial work indices have been tested in several clinical entities. Recently, Galli et al. [35] demonstrated the value of GWW and GWI in providing details on dyssynchronous contraction and segmental work. The authors [35] identified, that responders to cardiac resynchronization therapy have a higher GCW than non-responders. Using GWI and GWW enabled the early identification of patients with acute coronary occlusion with non-ST-elevation [4]. Ischemia induces changes in myocardial contraction, and it has been shown that patients with subclinical ischemia have a dyssynchronous contraction and increased GWW [14].

Secondary right ventricular failure can aggravate cardiogenic shock [36, 37]. Thus, prevention of right ventricular distension might play a crucial role in limiting progression to right ventricular failure, even during intravascular resuscitation [37]. Notably, the right ventricular preload is increased during left ventricular mechanical support [38]. Transvalvular LV pumps depend on left ventricular preload to prevent

suction and allow for optimal flows [38, 39]. Reduction in right ventricular afterload by pulmonary vasodilatation, leading to a decrease in pulmonary vascular resistance, should facilitate the reduction of left ventricular filling and right ventricular myocardial workload [40, 41]. The results of this study confirmed that iNO successfully decreases right ventricular afterload, normalizes RV filling pressure over time, and shifts the RV strain towards a normal (i.e., baseline) configuration.

Limitations

The small sample size of the study limits the significance of our analysis as it was not adequately powered for multiple comparisons. However, from an ethical perspective, the downsizing of experimental groups is part of the 3R strategy. The TEE measurements in swine are challenging due to specific anatomic features. Special attention was paid to avoid foreshortening of the left ventricle in echocardiography, and ante- and retroflexion of the tip was used to correctly identify the apex of the heart. Despite all the precautions, foreshortened ventricle views might have underestimated the left ventricular volumes including the stroke volume, RV D_3 and RV areas. 3D-TEE is believed to overcome these limitations and would have led to a more precise calculation of the derived parameters. The image quality of two-chamber-views can be limited due to swine anatomy (the bronchus partially conceals the heart from the esophagus). There are no studies comparing RV PS-loops with invasive PV-loops, to the best of our knowledge, due to lack of specific software for RV myocardial work assessment. We used the commercially available LV software provided by GE for RV myocardial work measurements. Therefore, the results must be interpreted with caution. The peripheral arterial pressure was used for PS-loop evaluation, which might be lower than the central arterial due to a lack of pressure augmentation.

Conclusions

During resuscitation from cardiac arrest, iCPR provides sufficient unloading and preservation of end-organ perfusion by maintaining cardiac output and improving myocardial work recovery. The addition of inhaled nitric oxide enables improved preservation of RV function as determined by better recovery of RV global work indices. Myocardial work estimation by echocardiographic analysis can help understand and guide both left and right ventricular unloading to minimize myocardial stress and oxygen demand, while maintaining sufficient end-organ perfusion.

Abbreviations

CA: Cardiac arrest

CO_{PWD}: Cardiac output as measured by pulsed-wave Doppler

CO_{TD}: Cardiac output measured with thermodilution method using Swan-Ganz catheter

DBP: Diastolic blood pressure

DPAP: Diastolic pulmonary artery pressure

GCW: Global constructed myocardial work

GLS: Global longitudinal strain

GWE: Global myocardial work efficiency

GWI: Global myocardial work index;

GWW: Global wasted work

HR: Heart rate

$HR_{pp-VF} \text{ min}^{-1}$: peak to peak inspiration frequency as the heart rate during cardiac arrest

iCPR: Percutaneous mechanical cardiopulmonary resuscitation

iNO: Inhaled nitric oxide

LAX: apical long axes view

LV: Left ventricle

LVEDV: Left ventricular end-diastolic volume

LVEF: Left ventricular ejection fraction

LVEDP: Left ventricular diastolic pressure

LVOT: Left ventricular outflow tracts

PSL: Pressure strain loop

PV-loop: Pressure-volume loop

PWD: Pulsed-wave Doppler

ROSC: Return of spontaneous circulation

RV: Right ventricle

RVEDD: Right ventricular end-diastolic diameter

RVEDP: Right ventricular diastolic pressure

RVD1: Right ventricle basal diameter

RVD2: mid right ventricle diameter

RV3: longitudinal right ventricle diameter

RV-FAC: Right ventricular fractional area change

RVOT: Right ventricular outflow tracts

SBP: Systolic blood pressure

SPAP: Systolic pulmonary artery pressure

STE: 2-D speckle-tracking echocardiography

TASV: Tricuspid annular systolic velocity

TDI: Tissue Doppler imaging

TEE: Transesophageal echocardiography

VTI: Velocity time integrals

Declarations

Ethics approval and consent to participate: The experimental protocol was approved by the appropriate governmental institution (Landesamt für Natur, Umwelt und Verbraucherschutz NRW (LANUV), Recklinghausen, Germany) Az.: 84-02.04.2017.A300

Consent for publication: Not applicable

Availability of data and materials: The datasets used or analyzed during the current study are available from the corresponding author on reasonable request.

Competing interests: AG and CN are full-time employee of Abiomed Europe GmbH, Germany. UM is a full-time employee Inc., USA. All other authors declare no competing interests

Funding: This work was supported by the German Research Foundation (Deutsche Forschungsgemeinschaft, DFG) [Grant Number DE 1685/3-1]. MD received unrestricted educational research grants and travel allowances from Abiomed Europe. The sponsor was not involved in study design; in the collection, analysis and interpretation of data; in the writing of the report; and in the decision to submit the article for publication.

Authors' contributions:

CN wrote and drafted the manuscript

CN, MD, NH, RR conception and Study design

CN, AE, AG, MD, RZ carried out the experiments, participated in the data acquisition

RZ, NH performed and analyzed the echocardiographic studies

CN, AE, NH, RZ collected and analyzed the data

AG, MD, NH, RR, UM Interpretation of the analysis

All authors critically revised the manuscript for important intellectual content

All authors have approved the submitted version

Acknowledgements not applicable

Authors' information not applicable

References

1. Derwall M, Brücken A, Bleilevens C, Ebeling A, Föhr P, Rossaint R, Kern KB, Nix C, Fries M: Doubling survival and improving clinical outcomes using a left ventricular assist device instead of chest compressions for resuscitation after prolonged cardiac arrest: a large animal study. *Crit Care* 2015, 19(1):123.
2. Derwall M, Ebeling A, Nolte KW, Weis J, Rossaint R, Ichinose F, Nix C, Fries M, Brücken A: Inhaled nitric oxide improves transpulmonary blood flow and clinical outcomes after prolonged cardiac arrest: a large animal study. *Crit Care* 2015, 19(1):328.
3. Curran J, Burkhoff D, Kloner RA: Beyond Reperfusion: Acute Ventricular Unloading and Cardioprotection During Myocardial Infarction. *J Cardiovasc Transl Res* 2019, 12(2):95-106.
4. Boe E, Russell K, Eek C, Eriksen M, Remme EW, Smiseth OA, Skulstad H: Non-invasive myocardial work index identifies acute coronary occlusion in patients with non-ST-segment elevation-acute coronary syndrome. *European heart journal cardiovascular Imaging* 2015, 16(11):1247-1255.
5. Al-Rashid F, Nix C, Erbel R, Kahlert P: Tools & Techniques - clinical: percutaneous catheter-based left ventricular support using the Impella CP. *EuroIntervention* 2015, 10(10):1247-1249.
6. Billig S, Zayat R, Ebeling A, Steffen H, Nix C, Hatam N, Schnöring H, Derwall M: Transesophageal echocardiography in swine: evaluation of left and right ventricular structure, function and myocardial work. *The international journal of cardiovascular imaging* 2020.
7. Flachskampf FA, Wouters PF, Edvardsen T, Evangelista A, Habib G, Hoffman P, Hoffmann R, Lancellotti P, Pepi M: Recommendations for transoesophageal echocardiography: EACVI update 2014. *European heart journal cardiovascular Imaging* 2014, 15(4):353-365.
8. Lang RM, Badano LP, Mor-Avi V, Afilalo J, Armstrong A, Ernande L, Flachskampf FA, Foster E, Goldstein SA, Kuznetsova T *et al*: Recommendations for cardiac chamber quantification by

- echocardiography in adults: an update from the American Society of Echocardiography and the European Association of Cardiovascular Imaging. *J Am Soc Echocardiogr* 2015, 28(1):1-39 e14.
9. Rudski LG, Lai WW, Afilalo J, Hua L, Handschumacher MD, Chandrasekaran K, Solomon SD, Louie EK, Schiller NB: Guidelines for the echocardiographic assessment of the right heart in adults: a report from the American Society of Echocardiography endorsed by the European Association of Echocardiography, a registered branch of the European Society of Cardiology, and the Canadian Society of Echocardiography. *J Am Soc Echocardiogr* 2010, 23(7):685-713; quiz 786-688.
 10. Russell K, Eriksen M, Aaberge L, Wilhelmsen N, Skulstad H, Gjesdal O, Edvardsen T, Smiseth OA: Assessment of wasted myocardial work: a novel method to quantify energy loss due to uncoordinated left ventricular contractions. *Am J Physiol Heart Circ Physiol* 2013, 305(7):H996-1003.
 11. Russell K, Eriksen M, Aaberge L, Wilhelmsen N, Skulstad H, Remme EW, Haugaa KH, Opdahl A, Fjeld JG, Gjesdal O *et al*: A novel clinical method for quantification of regional left ventricular pressure-strain loop area: a non-invasive index of myocardial work. *Eur Heart J* 2012, 33(6):724-733.
 12. Hubert A, Le Rolle V, Leclercq C, Galli E, Samset E, Casset C, Mabo P, Hernandez A, Donal E: Estimation of myocardial work from pressure-strain loops analysis: an experimental evaluation. *European heart journal cardiovascular Imaging* 2018, 19(12):1372-1379.
 13. Previtro M, Azzolina D, Palermo C, Tenaglia RM, Sammarco G, Ruozi N, Aruta P, Iliceto S, Muraru D, Badano L: ROLE OF NON-INVASIVE LEFT VENTRICULAR PRESSURE-STRAIN LOOP TO PREDICT CARDIAC DEATH AND ARRHYTHMIC RISK IN PATIENT WITH ORGANIC HEART DISEASE AND REDUCED LEFT VENTRICULAR EJECTION FRACTION. *Journal of the American College of Cardiology* 2019, 73(9 Supplement 1):1625.
 14. Lustosa RP, van der Bijl P, El Mahdiui M, Montero-Cabezas JM, Kostyukevich MV, Ajmone Marsan N, Bax JJ, Delgado V: Noninvasive Myocardial Work Indices 3 Months after ST-Segment Elevation Myocardial Infarction: Prevalence and Characteristics of Patients with Postinfarction Cardiac Remodeling. *J Am Soc Echocardiogr* 2020.
 15. Haugaa KH, Grenne BL, Eek CH, Ersbøll M, Valeur N, Svendsen JH, Florian A, Sjøli B, Brunvand H, Køber L *et al*: Strain echocardiography improves risk prediction of ventricular arrhythmias after myocardial infarction. *JACC Cardiovascular imaging* 2013, 6(8):841-850.
 16. Zhao H, Lee AP, Li Z, Qiao Z, Fan Y, An D, Xu J, Pu J, Shen X, Ge H *et al*: Impact of Intramyocardial Hemorrhage and Microvascular Obstruction on Cardiac Mechanics in Reperfusion Injury: A Speckle-Tracking Echocardiographic Study. *J Am Soc Echocardiogr* 2016, 29(10):973-982.
 17. Hammoudi N, Watanabe S, Bikou O, Ceccaldi A, Fish K, Yamada KP, Miyashita S, Lebreton G, Hajjar RJ, Ishikawa K: Speckle-Tracking Echocardiographic Strain Analysis Reliably Estimates Degree of Acute LV Unloading During Mechanical LV Support by Impella. *J Cardiovasc Transl Res* 2019, 12(2):135-141.
 18. Hedwig F, Soltani S, Stein J, Schoenrath F, Potapov E, Knosalla C, Falk V, Knebel F, Knierim J: Global work index correlates with established prognostic parameters of heart failure. *Echocardiography (Mount Kisco, NY)* 2020, 37(3):412-420.

19. Vonk-Noordegraaf A, Westerhof N: Describing right ventricular function. *European Respiratory Journal* 2013, 41(6):1419-1423.
20. Houard L, Benaets MB, de Meester de Ravenstein C, Rousseau MF, Ahn SA, Amzulescu MS, Roy C, Slimani A, Vancraeynest D, Pasquet A *et al*: Additional Prognostic Value of 2D Right Ventricular Speckle-Tracking Strain for Prediction of Survival in Heart Failure and Reduced Ejection Fraction: A Comparative Study With Cardiac Magnetic Resonance. *JACC Cardiovascular imaging* 2019, 12(12):2373-2385.
21. Lejeune S, Roy C, Ciocea V, Slimani A, de Meester C, Amzulescu M, Pasquet A, Vancraeynest D, Beauloye C, Vanoverschelde JL *et al*: Right Ventricular Global Longitudinal Strain and Outcomes in Heart Failure with Preserved Ejection Fraction. *J Am Soc Echocardiogr* 2020, 33(8):973-984.e972.
22. Perkins GD, Olasveengen TM, Maconochie I, Soar J, Wyllie J, Greif R, Lockey A, Semeraro F, Van de Voorde P, Lott C *et al*: European Resuscitation Council Guidelines for Resuscitation: 2017 update. *Resuscitation* 2018, 123:43-50.
23. BERGLUND E, MONROE RG, SCHREINER GL: Myocardial Oxygen Consumption and Coronary Blood Flow during Potassium-Induced Cardiac Arrest and during Ventricular Fibrillation¹. *Acta Physiologica Scandinavica* 1957, 41(2-3):261-268.
24. Sandroni C, Cavallaro F, Antonelli M: Is there still a place for vasopressors in the treatment of cardiac arrest? *Crit Care* 2012, 16(2):213.
25. Kapur NK, Reyelt L, Swain L, Esposito M, Qiao X, Annamalai S, Meyns B, Smalling R: Mechanical Left Ventricular Unloading to Reduce Infarct Size During Acute Myocardial Infarction: Insight from Preclinical and Clinical Studies. *J Cardiovasc Transl Res* 2019, 12(2):87-94.
26. Kapur NK, Paruchuri V, Urbano-Morales JA, Mackey EE, Daly GH, Qiao X, Pandian N, Perides G, Karas RH: Mechanically Unloading the Left Ventricle Before Coronary Reperfusion Reduces Left Ventricular Wall Stress and Myocardial Infarct Size. *Circulation* 2013, 128(4):328-336.
27. Saku K, Kakino T, Arimura T, Sakamoto T, Nishikawa T, Sakamoto K, Ikeda M, Kishi T, Ide T, Sunagawa K: Total Mechanical Unloading Minimizes Metabolic Demand of Left Ventricle and Dramatically Reduces Infarct Size in Myocardial Infarction. *PloS one* 2016, 11(4):e0152911.
28. Saku K, Kakino T, Arimura T, Sunagawa G, Nishikawa T, Sakamoto T, Kishi T, Tsutsui H, Sunagawa K: Left Ventricular Mechanical Unloading by Total Support of Impella in Myocardial Infarction Reduces Infarct Size, Preserves Left Ventricular Function, and Prevents Subsequent Heart Failure in Dogs. *Circulation Heart failure* 2018, 11(5):e004397.
29. Suga H: Ventricular energetics. *Physiol Rev* 1990, 70(2):247-277.
30. Suga H: Total mechanical energy of a ventricle model and cardiac oxygen consumption. *The American journal of physiology* 1979, 236(3):H498-505.
31. Burkhoff D, Mirsky I, Suga H: Assessment of systolic and diastolic ventricular properties via pressure-volume analysis: a guide for clinical, translational, and basic researchers. *Am J Physiol Heart Circ Physiol* 2005, 289(2):H501-512.

32. Bonnet B, Jourdan F, du Cailar G, Fesler P: Noninvasive evaluation of left ventricular elastance according to pressure-volume curves modeling in arterial hypertension. *Am J Physiol Heart Circ Physiol* 2017, 313(2):H237-h243.
33. Konstam MA, Abboud FM: Ejection Fraction: Misunderstood and Overrated (Changing the Paradigm in Categorizing Heart Failure). *Circulation* 2017, 135(8):717-719.
34. Mor-Avi V, Lang RM, Badano LP, Belohlavek M, Cardim NM, Derumeaux G, Galderisi M, Marwick T, Nagueh SF, Sengupta PP *et al*: Current and evolving echocardiographic techniques for the quantitative evaluation of cardiac mechanics: ASE/EAE consensus statement on methodology and indications endorsed by the Japanese Society of Echocardiography. *European journal of echocardiography : the journal of the Working Group on Echocardiography of the European Society of Cardiology* 2011, 12(3):167-205.
35. Galli E, Leclercq C, Hubert A, Bernard A, Smiseth OA, Mabo P, Samset E, Hernandez A, Donal E: Role of myocardial constructive work in the identification of responders to CRT. *European heart journal cardiovascular Imaging* 2018, 19(9):1010-1018.
36. Cinotti R, Léopold V, Mebazaa A: A Right Insight in Cardiogenic Shock to Get It Right. *J Card Fail* 2018, 24(3):157-158.
37. Schoenrath F, Hoch D, Maisano F, Starck CT, Seifert B, Wenger U, Ruschitzka F, Wilhelm MJ: Survival, quality of life and impact of right heart failure in patients with acute cardiogenic shock treated with ECMO. *Heart & lung : the journal of critical care* 2016, 45(5):409-415.
38. Kapur NK, Langston P, Esposito ML, Burkhoff D: Abrupt development of a trans-aortic valve gradient in the setting of acute left-sided circulatory support identifies right heart failure in cardiogenic shock: The Kapur-Langston sign. *Cardiovasc Revasc Med* 2020.
39. Mandawat A, Rao SV: Percutaneous Mechanical Circulatory Support Devices in Cardiogenic Shock. *Circ Cardiovasc Interv* 2017, 10(5).
40. Kapur NK, Esposito ML, Bader Y, Morine KJ, Kiernan MS, Pham DT, Burkhoff D: Mechanical Circulatory Support Devices for Acute Right Ventricular Failure. *Circulation* 2017, 136(3):314-326.
41. Zayat R, Ahmad U, Stoppe C, Khattab MA, Arab F, Moza A, Tewarie L, Goetzenich A, Autschbach R, Schnoering H: Sildenafil Reduces the Risk of Thromboembolic Events in HeartMate II Patients with Low-Level Hemolysis and Significantly Improves the Pulmonary Circulation. *Int Heart J* 2018, 59(6):1227-1236.

Tables

Table 1. Hemodynamic parameters before, during and after the resuscitation using a percutaneous mechanical circulatory support device.

	<i>0ppm</i>	<i>20ppm</i>	<i>Total</i>	<i>p</i>
<i>BSA m²</i>	1.2±0.1	1.3±0.1	1.3±0.1	0.271
Baseline				
<i>HR min⁻¹</i>	85.6±13.9	98.4±11.6	92.0±13.8	0.152
<i>SBP mmHg</i>	129.2±16.5	126.4±20.3	127.8±17.5	0.817
<i>DBP mmHg</i>	68.6±8.6	67.4±5.9	68.0±7.0	0.805
<i>SPAP mmHg</i>	26.6±2.8	24.8±3.6	25.7±3.2	0.400
<i>DPAP mmHg</i>	14.2±2.7	12.4±2.9	13.3±2.8	0.337
<i>CO_{PWD} L/min</i>	6.9±1.7	7.0±0.8	7.0±1.3	0.878
<i>CO_{TD} L/min</i>	6.7±1.5	7.3±0.7	7.0±1.2	0.459
Cardiac arrest				
<i>CO_{PWD} L/min</i>	1.7±0.2	1.8±0.2	1.8±0.2	0.341
<i>Impella flow L/min</i>	1.9±0.3	1.9±0.2	1.9±0.2	0.892
<i>HR_{pp-VF} min⁻¹</i>	20.8±1.1	21.4±0.8	21.1±0.9	0.491
30min post-ROSC				
<i>HR min⁻¹</i>	115±24.3	130±30	128±36	0.055
<i>SBP mmHg</i>	95.2±12.9	95.6±25.1	95.4±18.8	0.976
<i>DBP mmHg</i>	64.8±10.6	64.4±10.9	64.6±10.1	0.955
<i>SPAP mmHg</i>	26.2±3.8	25.2±6.2	25.7±4.9	0.766
<i>DPAP mmHg</i>	14.4±3.5	11.8±5.3	13.1±4.5	0.388
<i>CO_{TD} L/min</i>	5.5±1.7	5.6±1.2	5.6±1.4	0.900
<i>CO_{PWD} L/min</i>	5.1±1.1	5.7±1.2	5.4±1.1	0.433
3h post-ROSC				
<i>HR min⁻¹</i>	102.8±13.9	111.6±21.6	107.2±17.7	0.466
<i>SBP mmHg</i>	99.6±8.6	114.2±28.0	106.9±21.0	0.298
<i>DBP mmHg</i>	68.0±7.3	65.0±11.7	66.5±9.3	0.639
<i>SPAP mmHg</i>	28.0±5.5	28.4±4.6	28.2±4.8	0.903

<i>DPAP mmHg</i>	15.0±3.2	14.4±3.6	14.7±3.3	0.790
<i>CO_{PWD} L/min</i>	4.6±1.0	6.6±1.1	5.7±1.5	0.016
<i>CO_{TD} L/min</i>	5.1±0.8	6.8±2.3	5.9±1.8	0.172
5h post-ROSC				
<i>HR min⁻¹</i>	75.0±11.0	104.8±19.6	89.9±21.7	0.018
<i>SBP mmHg</i>	110.2±13.8	113.0±18.0	111.6±15.2	0.790
<i>DBP mmHg</i>	68.0±9.8	66.2±9.0	67.1±8.9	0.771
<i>SPAP mmHg</i>	32.0±4.4	23.0±1.0	27.5±5.6	0.008
<i>DPAP mmHg</i>	16.2±3.7	11.8±1.3	14.0±3.5	0.037
<i>CO_{PWD} L/min</i>	4.0±0.6	5.8±1.0	4.9±1.2	0.036
<i>CO_{TD} L/min</i>	3.5±0.6	5.6±1.5	4.5±1.6	0.021

CO_{PWD}: Pulsed- wave Doppler derived cardiac output; *CO_{TD}*: Cardiac output measured with thermodilution method using wan-Ganz catheter; DBP: Diastolic blood pressure; DPAP: Diastolic pulmonary artery pressure; HR: Heart rate; *HR_{pp-VF}*: Peak to peak ventilation frequency as the Heart rate during cardiac arrest; SBP: Systolic blood pressure; SPAP: Systolic pulmonary artery pressure

Table 2: Comparison of echocardiographic parameters between the groups with and without inhaled nitric oxide.

	<i>0ppm</i>	<i>20ppm</i>	<i>Total</i>	<i>p</i>
Baseline				
<i>RVD1 cm</i>	3.1±0.4	3.4±0.4	3.3±0.4	0.332
<i>RVD2 cm</i>	2.6±0.2	2.7±0.4	2.6±0.3	0.417
<i>RVD3 cm</i>	4.0±0.2	3.8±0.4	3.9±0.3	0.424
<i>RV-FAC %</i>	44.1±6.0	42.9±6.6	43.5±6.0	0.772
<i>LVEDV mL</i>	70.5±3.5	70.9±6.1	70.7±4.7	0.911
<i>LVESV mL</i>	31.9±4.6	33.4±3.6	32.6±4.0	0.583
<i>LV-EF %</i>	61.5±5.8	64.7±9.2	63.1±7.5	0.525
<i>LV-GLS %</i>	-21.0±5.1	-21.6±3.4	-21.3±4.1	0.833
<i>LV-GWI mmHg%</i>	1835.3±306.2	1751±270.2	3444.3±5242.8	0.336
<i>LV-GCW mmHg%</i>	2095.8±527.4	2103.2±405.8	2099.5±443.6	0.981
<i>LV-GWW mmHg%</i>	368.0±208.8	352.4±115.9	360.2±159.4	0.887
<i>LV-GWE %</i>	85.2±4.7	80.0±1.4	82.6±4.2	0.054
<i>TASV cm/sec.</i>	13.6±1.1	13.8±1.5	13.7±1.3	0.817
<i>RV-GLS %</i>	-16.4±3.2	-14.4±1.8	-15.4±2.7	0.267
<i>RV-GWI mmHg%</i>	338.2±45.3	286.8±57.5	312.5±55.8	0.155
<i>RV-GCW mmHg%</i>	376.4±92.6	266.6±41.1	321.5±89.0	0.082
<i>RV-GWW mmHg%</i>	61.6±13.8	55.4±10.6	58.5±12.1	0.949
<i>RV-GWE %</i>	79.8±10.2	80.8±6.1	80.3±7.9	0.855
Cardiac arrest				
<i>RVD1 cm</i>	4.0±0.3	4.2±0.3	4.1±0.3	0.397
<i>RVD2 cm</i>	3.3±0.6	3.5±0.4	3.4±0.5	0.581
<i>RVD3 cm</i>	4.5±0.2	4.6±0.5	4.6±0.4	0.749
<i>RVEDA cm²</i>	13.9±1.6	15.2±1.1	14.6±1.4	0.183
<i>LVEDV mL</i>	81.0±4.9	76.6±7.5	78.8±6.4	0.306
30min. post-ROSC				
<i>RVD1 cm</i>	3.7±0.3	3.6±0.4	3.7±0.3	0.582
<i>RVD2 cm</i>	3.0±0.4	2.9±0.4	2.9±0.4	0.716

<i>RVD3 cm</i>	4.5±0.2	4.6±0.1	4.5±0.2	0.776
<i>RV-FAC %</i>	27.4±2.8	32.0±9.3	30.5±6.5	0.494
<i>LVEDV mL</i>	77.0±6.5	73.8±9.7	75.4±8.0	0.558
<i>LVESV mL</i>	35.8±5.1	35.4±3.7	35.6±4.2	0.897
<i>LVEF %</i>	47.6±5.0	42.0±8.1	44.8±7.0	0.225
<i>LV-GLS %</i>	-11.6±3.3	-13.2±4.7	-12.4±3.9	0.548
<i>LV-GWI mmHg%</i>	891.2±412.7	1201.8±400.5	1046.5±416.8	0.262
<i>LV-GCW mmHg%</i>	719.0±497.8	919.6±638.2	819.3±549.8	0.595
<i>LV-GWW mmHg%</i>	360.4±271.1	240.2±148.1	300.3±215.4	0.416
<i>LV-GWE %</i>	63.4±7.7	75.0±8.7	69.2±9.9	0.256
<i>TASV cm/sec.</i>	10.4±4.9	9.8±1.8	10.1±3.5	0.803
<i>RV-GLS %</i>	-6.6±3.3	-9.4±2.9	-8.0±3.3	0.193
<i>RV-GWI mmHg%</i>	101.6±34.5	92.0±33.3	96.8±32.4	0.666
<i>RV-GCW mmHg%</i>	152.2±15.5	159.6±20.2	164.1±40.0	0.395
<i>RV-GWW mmHg%</i>	59.4±11.9	49.4±9.1	52.3±13.2	0.843
<i>RV-GWE %</i>	70.6±12.0	74.0±8.6	72.3±10.0	0.621
3h. post-ROSC				
<i>RVD1 cm</i>	3.3±0.3	3.4±0.3	3.4±0.3	0.782
<i>RVD2 cm</i>	2.7±0.3	2.8±0.1	2.8±0.2	0.347
<i>RVD3 cm</i>	4.4±0.1	4.3±0.3	4.3±0.2	0.718
<i>RV-FAC %</i>	32.5±5.0	43.3±7.0	43.2±6.8	0.945
<i>LVEDV mL</i>	78.2±1.1	70.8±1.3	74.5±4.1	<0.001
<i>LVESV mL</i>	38.0±4.9	35.2±3.5	36.6±4.3	0.342
<i>LVEF %</i>	61.5±5.8	64.7±9.2	63.1±7.5	0.525
<i>LV-GLS %</i>	-12.2±2.8	-16.0±2.3	-14.1±3.1	0.058
<i>LV-GWI mmHg%</i>	896.2±129.3	1399.2±347.3	1147.7±362.4	0.116
<i>LV-GCW mmHg%</i>	719.0±497.8	1598.8±849.2	1158.9±803.5	0.081
<i>LV-GWW mmHg%</i>	264.6±78.9	293.4±212.5	279.0±151.9	0.784
<i>LV-GWE %</i>	67.2±3.3	81.4±5.6	74.3±8.7	0.010

<i>TASV cm/sec.</i>	7.8±1.6	11.4±1.1	11.0±1.5	0.024
<i>RV-GLS %</i>	-10.0±1.0	-12.0±2.7	-11.0±2.2	0.164
<i>RV-GWI mmHg%</i>	108.4±22.6	189.6±43.6	149.0±53.9	0.049
<i>RV-GCW mmHg%</i>	203.4±39.6	221.2±85.6	212.3±63.6	0.684
<i>RV-GWW mmHg%</i>	69.6±11.9	47.4±6.7	47.8±13.3	0.049
<i>RV-GWE %</i>	72.2±14.0	75.0±11.1	73.6±12.0	0.734
5h post-ROSC				
<i>RVD1 cm</i>	3.5±0.5	3.9±0.7	3.7±0.6	0.308
<i>RVD2 cm</i>	2.8±0.4	3.2±0.7	3.0±0.6	0.287
<i>RVD3 cm</i>	4.4±0.2	4.6±0.1	4.5±0.2	0.024
<i>RV-FAC %</i>	33.2±4.3	41.1±6.5	37.1±6.7	0.053
<i>LVEDV mL</i>	70.8±1.3	68.2±2.7	69.5±2.4	0.087
<i>LVESV mL</i>	38.0±6.9	35.6±4.5	36.8±5.6	0.525
<i>LVEF %</i>	51.4±3.0	57.0±6.2	54.2±5.5	0.108
<i>LV-GLS %</i>	-13.0±2.4	-18.2±3.4	-15.6±3.9	0.036
<i>LV-GWI mmHg%</i>	1125±214	1529.2±274.5	1251.3±348.4	0.052
<i>LV-GCW mmHg%</i>	1203.8±253.0	1728.4±466.7	1466.1±449.1	0.058
<i>LV-GWW mmHg%</i>	395.4±159.4	367.0±87.2	381.2±122.1	0.736
<i>LV-GWE %</i>	75.8±2.3	82.6±4.0	79.2±4.7	0.071
<i>TASV cm/s</i>	9.4±1.3	12.8±1.1	9.9±2.2	0.012
<i>RV-GLS %</i>	-9.0±1.4	-13.2±2.2	-11.1±2.8	0.040
<i>RV-GWI mmHg%</i>	152.6±42.4	261.6±54.2	207.1±73.5	0.041
<i>RV-GCW mmHg%</i>	224.4±158.7	212.6±53.8	218.5±111.9	0.879
<i>RV-GWW mmHg%</i>	77.8±14.8	50.2±8.2	61.4±22.4	0.046
<i>RV-GWE %</i>	68±5.7	80±5.2	76±5.4	0.042

GCW: Global constructed myocardial work; GLS: Global longitudinal strain; GWE: Global myocardial work efficiency; GWI: Global myocardial work index; GWW: Global wasted work; LV: Left ventricle; LVEDV: Left ventricle end-diastolic volume; LVEF: Left ventricular ejection fraction; LVESV: Left ventricular end-systolic volume; RVEDA: right ventricle end-diastolic area ; RVD1: right ventricle basal diameter from apical 4 chamber view; RVD2: right ventricular mid diameter at midlevel from apical 4 chamber view; RVD3: right

ventricle longitudinal diameter; RV-FAC: right ventricular fractional area change; TASV: Tricuspid annular systolic velocity

Figures

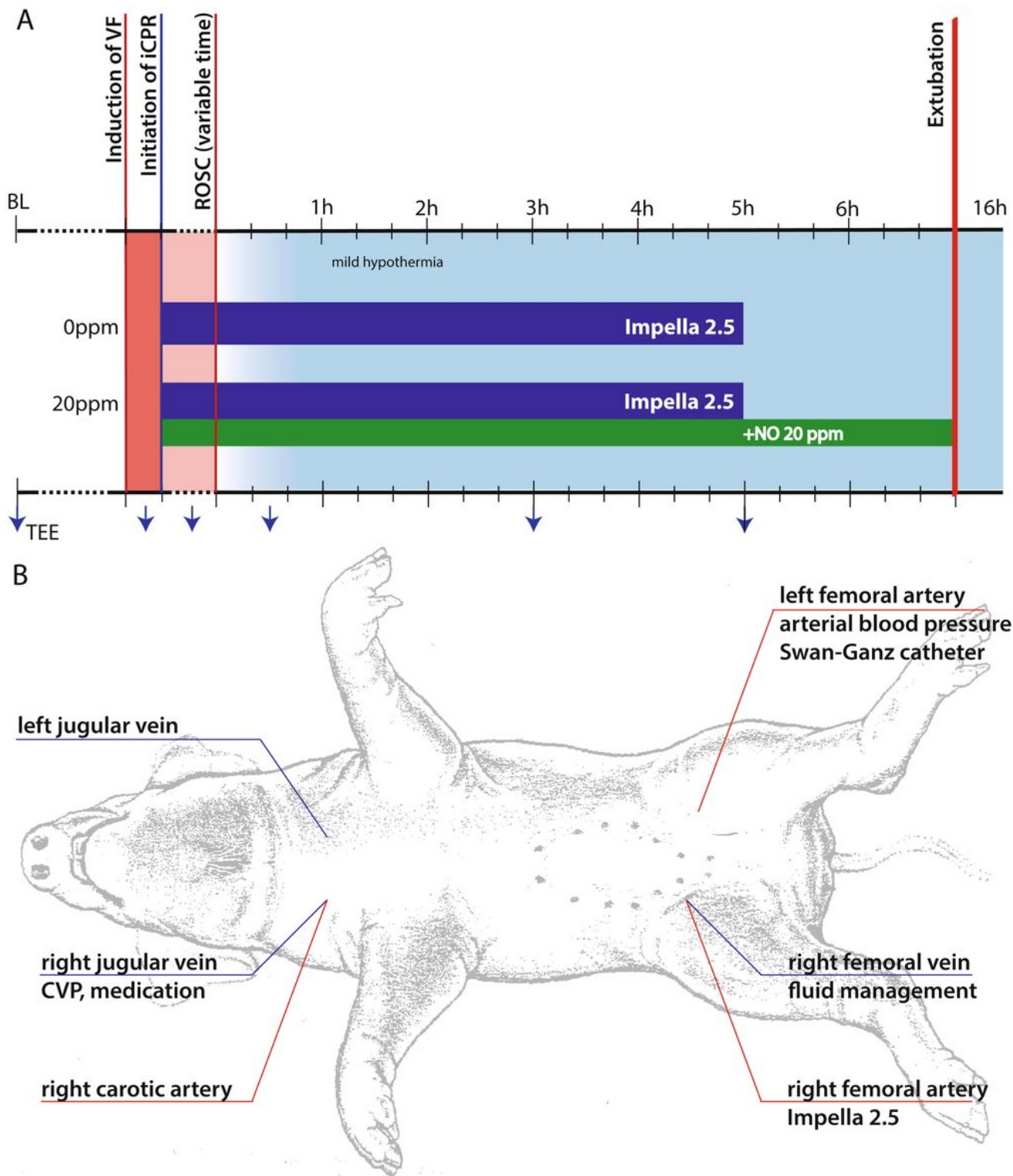


Figure 1

Experimental model (A) and instrumentation (B) CVP: central venous pressure; iCPR: Percutaneous mechanical cardiopulmonary resuscitation; VF: ventricular fibrillation; ROSC: Return of spontaneous circulation

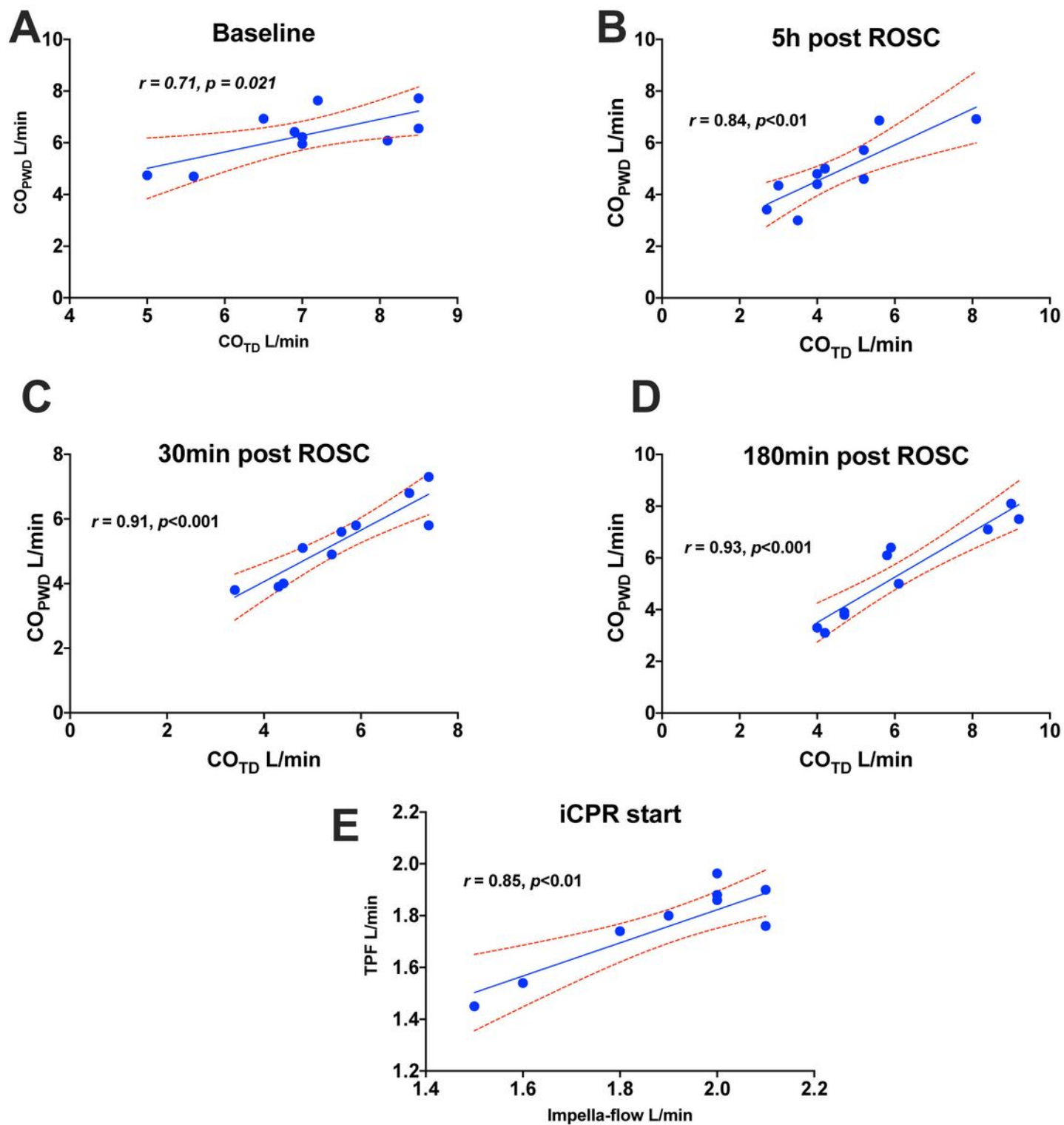


Figure 2

Cardiac output correlation between different methods of measurement. Comparison between cardiac output derived from pulsed-wave Doppler vs. thermodilution at different time-points (A, B, C, D) or vs.

Impella flow as shown on the automated Impella Controller during iCPR (E) in all animals (not separated by treatment group). Shown are the individual comparisons, linear correlation within a 95% confidence interval (red dotted line).

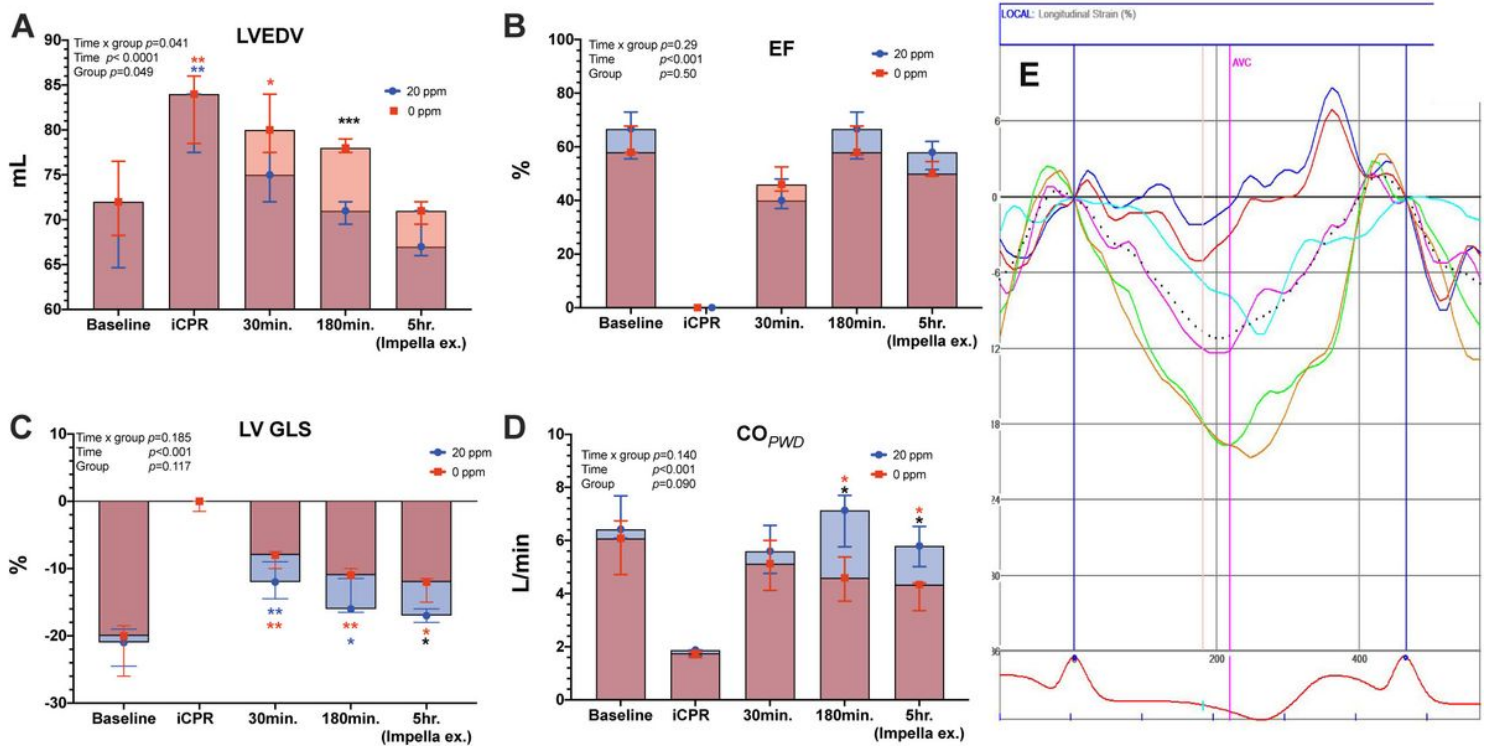


Figure 3

Time-course of left ventricular 2-dimensional echocardiographic parameters. A: Left ventricular end-diastolic volume (LVEDV); B: Left ventricular ejection fraction (EF); C: Left ventricular global longitudinal strain (LV GLS); D: Cardiac output as measured by pulsed-wave Doppler (CO_{pwd}); E: example of regional longitudinal strain analysis of the left ventricle. *: $p < 0.05$; **: $p < 0.01$; ***: $p < 0.001$. red asterisk: 0ppm group compared to baseline; blue asterisk: 20ppm group compared to baseline; black asterisk: between groups at specific time-point.

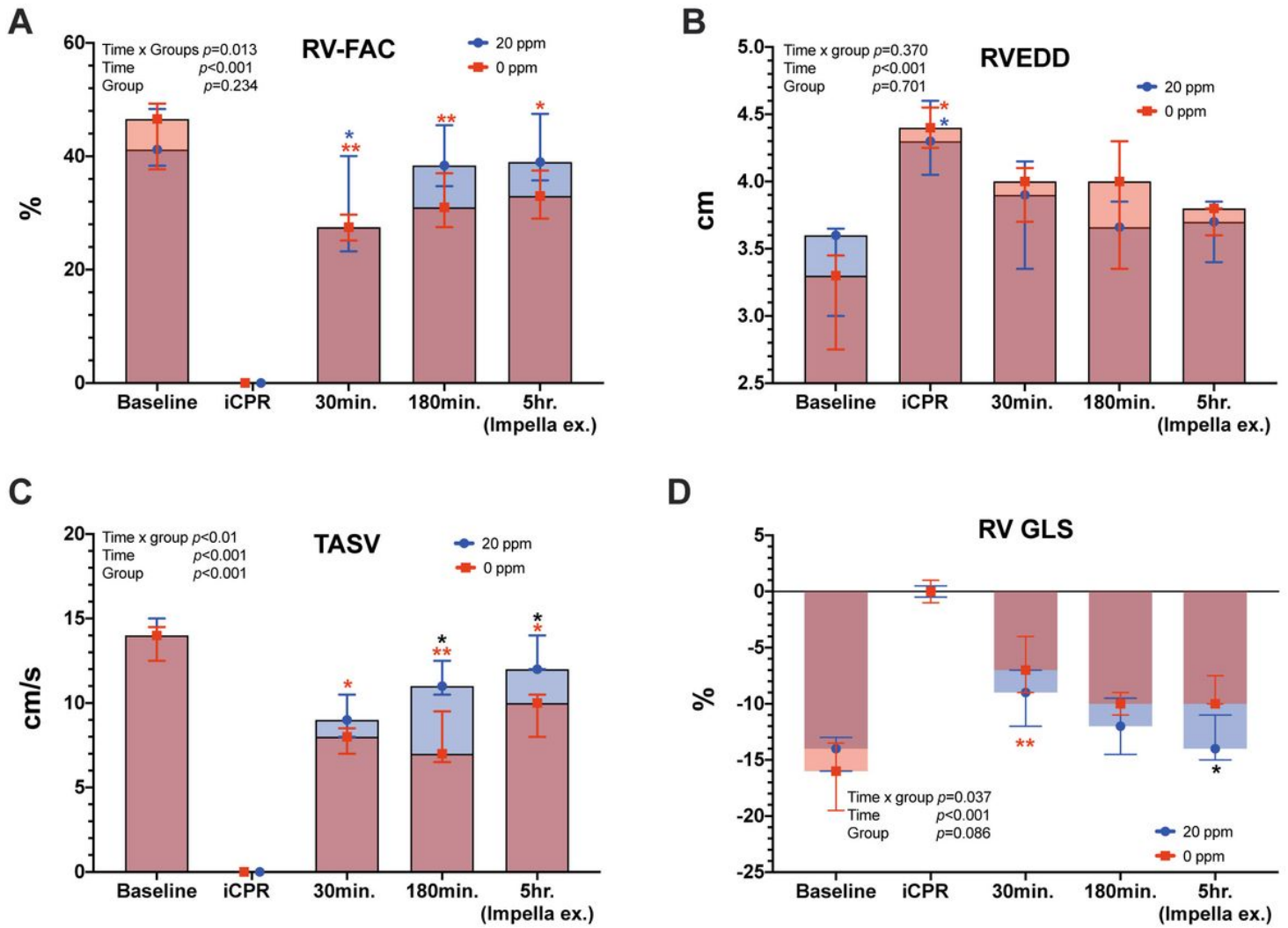


Figure 4

Time-course of right ventricular 2-dimensional echocardiographic parameters. A: Right ventricular fractional area change (RV-FAC); B: right ventricular end-diastolic diameter (RVEDD); C: tricuspid annular systolic velocity (TASV); D: right ventricular global longitudinal strain (RV GLS). *: $p<0.05$; **: $p<0.01$. Red asterisk: 0ppm group compared to baseline; blue asterisk: 20ppm group compared to baseline; black asterisk: between groups at specific time-point.

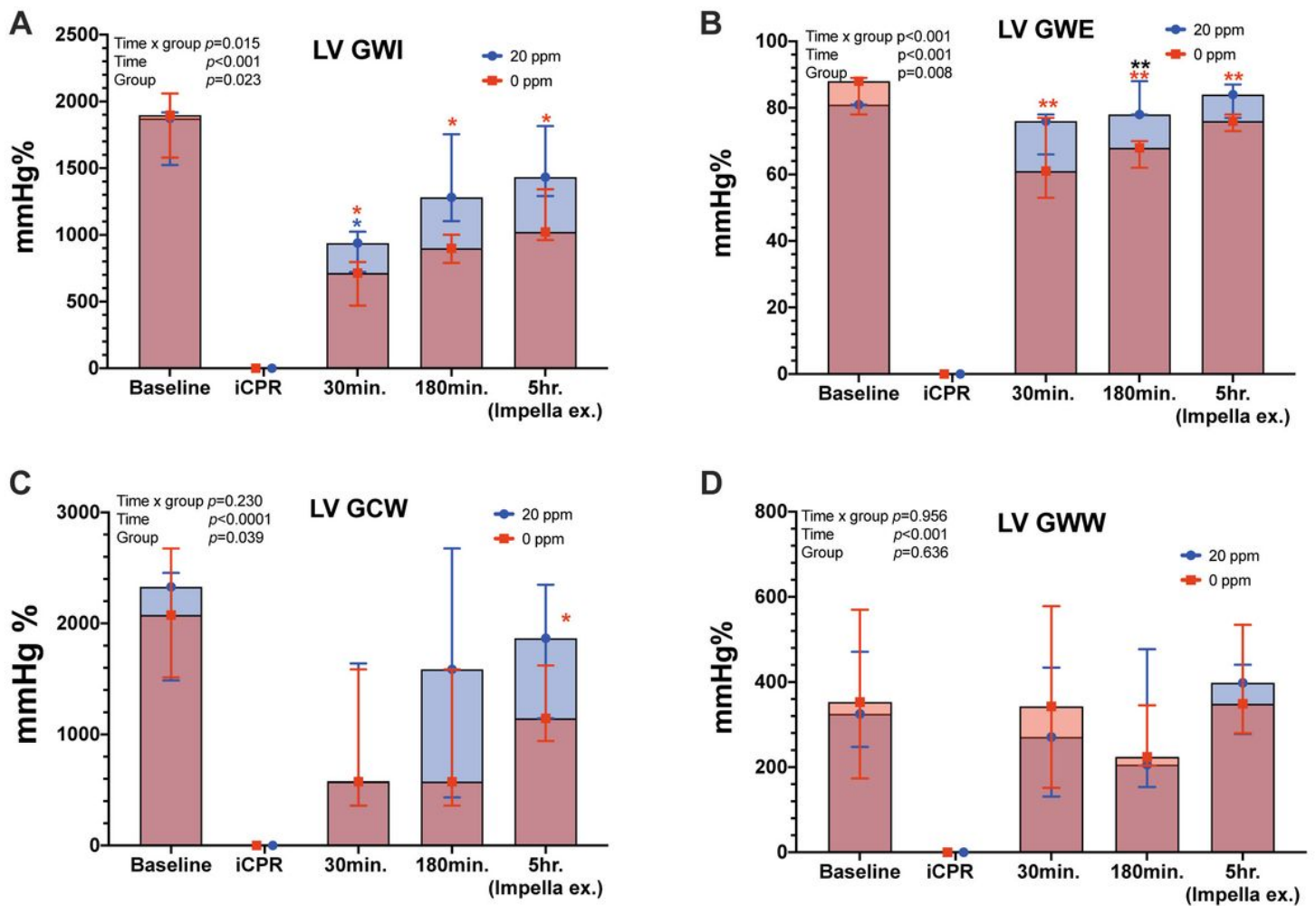


Figure 5

Changes of left ventricular function and myocardial work. A: Left ventricular global work index (LV GWI); B: Left ventricular global work efficiency (LV GWE); C: Left ventricular global constructed work (LV GCW); D: Left ventricular global wasted work (LV GWW). *: $p<0.05$; **: $p<0.01$. Red asterisk: 0ppm group compared to baseline; blue asterisk: 20ppm group compared to baseline; black asterisk: between groups at specific time-point.

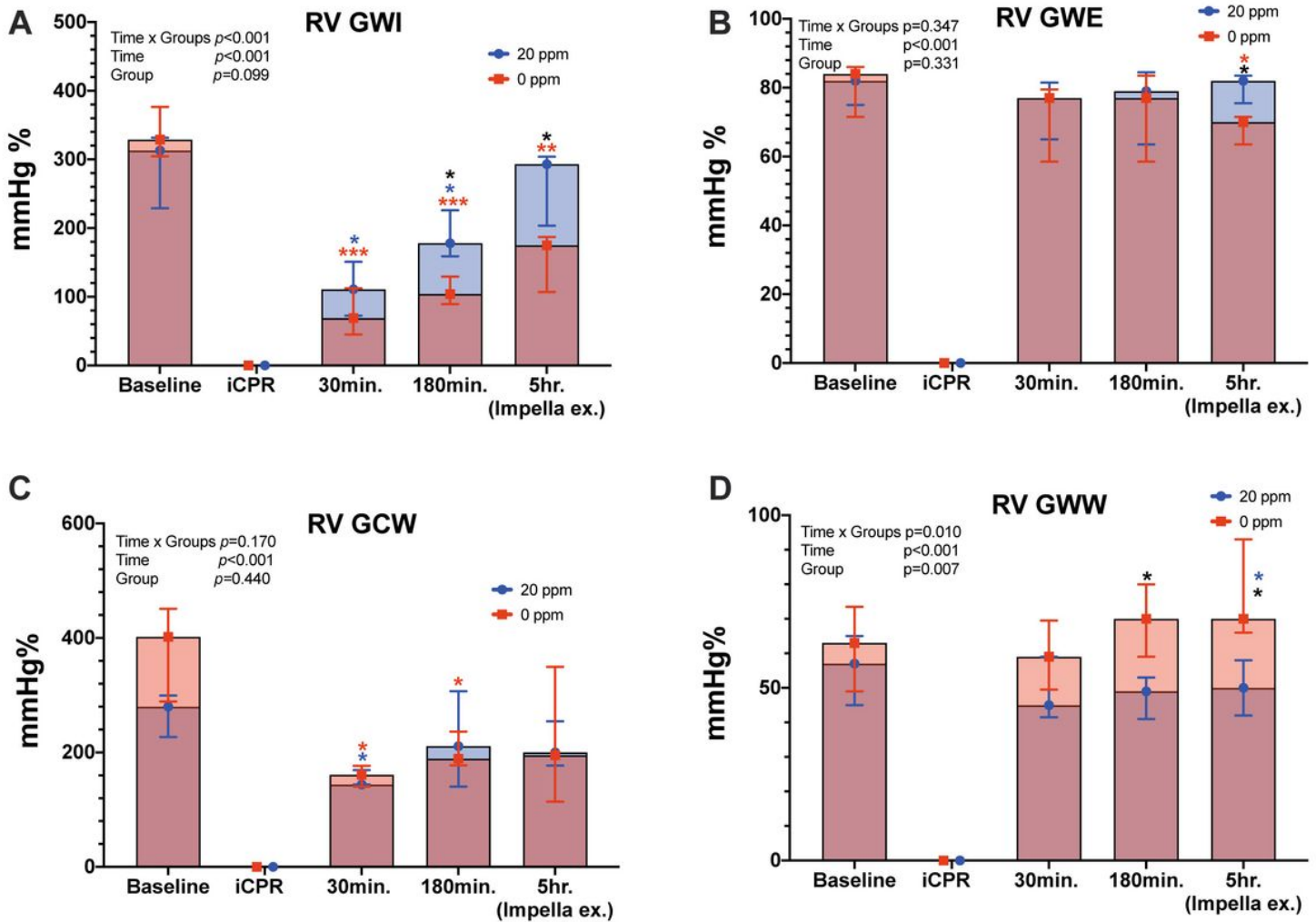


Figure 6

Changes of right ventricular function and myocardial work. A: Right ventricular global work index (RV GWI); B: Right ventricular global work efficiency (RV GWE); C: Right ventricular global constructed work (RV GCW); D: Right ventricular global wasted work (RV GWW). *: $p < 0.05$; **: $p < 0.01$; ***: $p < 0.001$. red asterisk: 0ppm group compared to baseline; blue asterisk: 20ppm group compared to baseline; black asterisk: between groups at specific time-point.

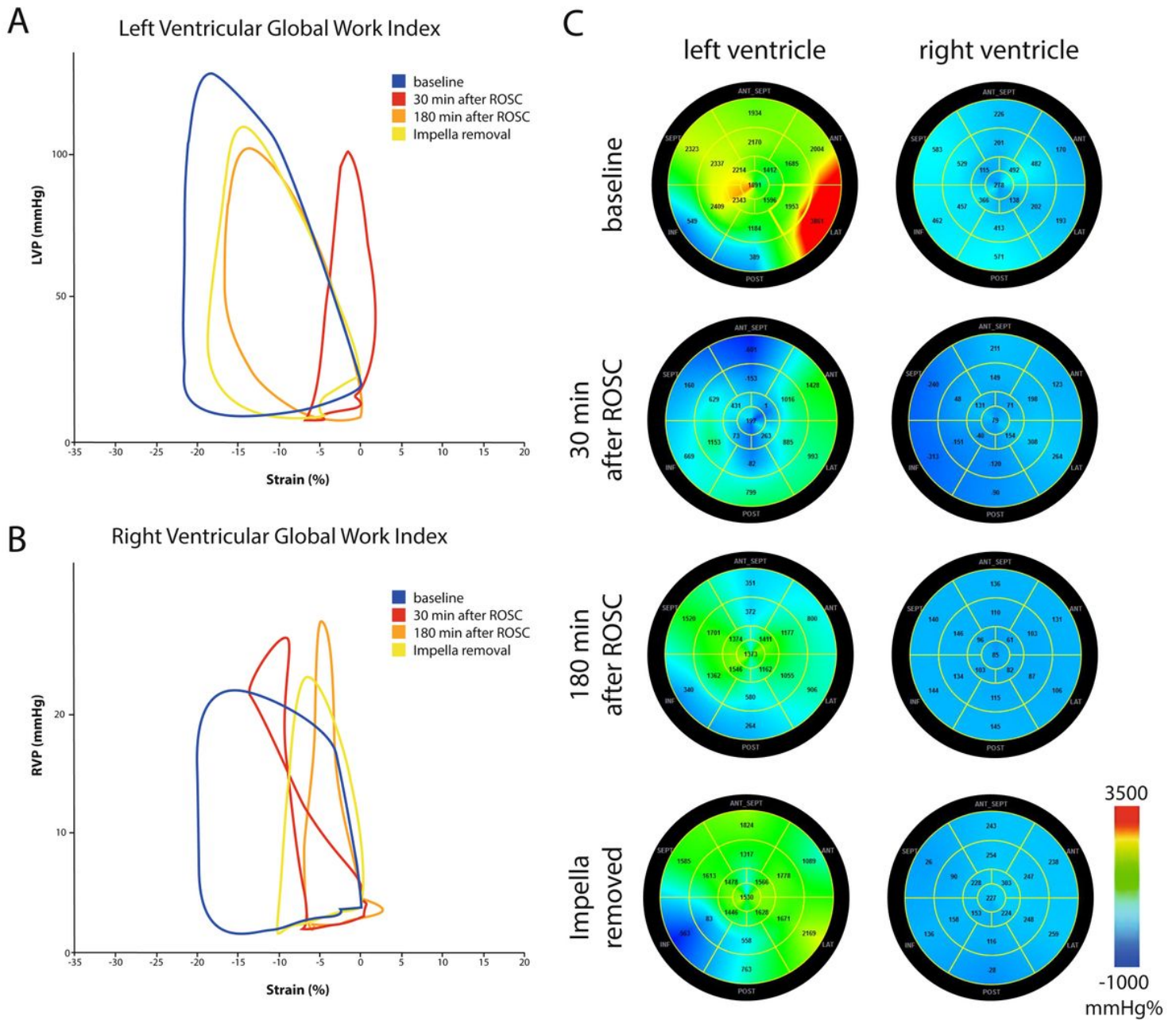


Figure 7

Exemplary demonstration of global myocardial work index changes during the experiment. A, B: relation of left/right ventricular pressure to global left/right ventricular strain over time. Comparable to a PV-loop, this allows to gain insights on myocardial workload and function. C: example of spatial distribution of right and left ventricular myocardial work index. Myocardial work indices are color coded from red to blue, where red color indicate the maximum value and blue the lowest myocardial work index value.

Supplementary Files

This is a list of supplementary files associated with this preprint. Click to download.

- [GraphicalAbstract.pdf](#)